

Near-IR adaptive optics imaging of nuclear spiral structure in the Seyfert galaxy, NGC 3227

Scott C. Chapman^{1,2,4}, Simon L. Morris^{3,4}, and Gordon A. H. Walker¹

[1] *Department of Physics & Astronomy, University of British Columbia, Vancouver, B.C. V6T 1Z4, Canada*

[2] *Present address: Observatories of the Carnegie Institution of Washington, Pasadena, CA 91101, U.S.A.*

[3] *Dominion Astrophysics Observatory, Victoria, B.C., Canada V8X 4M6*

[4] *Guest observer, Canada France Hawaii Telescope*

Accepted ... ; Received ... ; in original form ...

ABSTRACT

We present high spatial resolution, near-IR images in J , H , and K of the nucleus of NGC 3227, obtained with the Adaptive Optics bonnette on CFHT. The $\sim 0.15''$ (17pc) resolution allows structures to be probed in the core region. Dust obscuration becomes significantly less pronounced at longer wavelengths, revealing the true geometry of the core region. We are able to identify two main features in our maps: (*i*) a spiraling association of knots with a counterpart in an HST F606W image; (*ii*) a smaller scale annulus, orthogonal to the spiral of knots. These features may provide a means to transport material inwards to fuel the active nucleus.

Key words: galaxies: active – galaxies: starburst – galaxies: individual NGC3227

1 INTRODUCTION

It is generally accepted that pronounced activity in galaxies hosting Active Galactic Nuclei (AGN) results from accretion onto a supermassive black hole. However, the problems of overcoming the angular momentum barrier to fuel the nucleus (Shlosman et al. 1989) and also the unification of the AGN types (Antonucci 1993) continue to be vexing and controversial. Near-IR imaging has proven to be a powerful means to study these AGN problems, since the dust extinction is reduced, as is the contrast between the central AGN and the underlying stellar population (McLeod et al. 1995). A fresh perspective can be gained on the core regions of AGNs through the high resolution images now possible thanks to adaptive optics (AO).

Here, we present observations of NGC 3227 obtained with *PUEO*, the AO system recently commissioned on the 3.6 m Canada-France-Hawaii Telescope (Rigaut et al. 1998). NGC 3227 is an SABa galaxy, interacting with its dwarf elliptical neighbor, NGC 3226. It has been much studied in recent years as it contains many of the elements thought to be related to the formation and evolution of active nuclei: emission line regions excited by both starburst and AGN continuum, strong interaction, and a stellar bar (Gonzales Delgado & Perez 1997, Arribas & Mediavilla 1994).

2 OBSERVATIONS

The images were obtained at the CFHT in March, 1997, using the MONICA near-IR camera (Nadeau et al. 1994) mounted at the f/20 focus of the Adaptive Optics Bonnette (AOB). The detector is a Rockwell NICMOS3 array with 256×256 pixels and a $0.034''$ per pixel scale. The CFHT AOB is based on curvature wavefront sensing (Rodier 1991), and uses a 19 zone bimorph mirror to correct the wavefront distortions (Rigaut et al. 1998). As the field size is small with MONICA ($9'' \times 9''$), blank sky images were taken intermitantly between science frames. On-source images were taken in a mosaic of 4 positions, alternately putting the galaxy core in each of the four quadrants of the array. Flux and PSF calibrations were performed using the UKIRT standard stars fs13 and fs25. Flat-field images were taken on the dome with the lamps turned on and off to account for the thermal glow of the telescope. The nucleus of the galaxy itself was used as the guiding source for the AO system, roughly a 15th magnitude point source. The natural seeing averaged $0.6''$ - $0.8''$ throughout the observations resulting in relatively high strehl ratios in all bands, and FWHM of $0.14''$, $0.17''$, $0.22''$ at K , H , J bands respectively. At a distance of 15 Mpc for NGC 3227, $1'' = 76$ pc using $H_0 = 50 \text{ km s}^{-1} \text{ Mpc}^{-1}$.

Image processing proceeded as follows: *i*) bad pixel correction; *ii*) sky subtraction, using a median-averaged sky estimate; *iii*) flat-field correction; *iv*) re-centering of the different exposures through cross-correlation techniques; *v*) ad-

justment of the sky level among the overlapping regions to produce a homogeneous background; *vi*) co-addition of the overlapping regions, rejecting deviant pixels (clipped mean). The resulting images were then deconvolved using the classical Lucy-Richardson algorithm (25 iterations) with an input PSF reconstructed from the AO modal control commands obtained during the actual observations (Veran et al. 1997).

2.1 HST archive image

An HST WFPC2 image was retrieved from the archive for NGC3227 in the F606W filter, corresponding roughly to Johnson *V* and *R* bands. The strong $H\alpha$ line is contained in this filter, and can contribute as much as several percent to integrated flux in this band for some observed morphologies. The core of the galaxy lies on the PC chip with $0''.04$ pixels. The image was rotated and rebinned to match the pixel sampling and resolution of our AOB images. The core of the galaxy is actually saturated and CCD bleeding is seen lying along the NE-SW axis.

3 RESULTS

3.1 Core structures

The CFHT *J*, *H*, *K* and HST F606W (hereafter *V*) -band images are presented in figure 1, on a magnitude (log) scale. Subtraction of a smooth model galaxy (usually called *unsharp masking* – see below) reveals that this region is punctuated with bright knotty structures within a region $3'' \times 2''$ (figure 2). The knots appear to trace out several ring patterns, and are suggestive of a one-armed spiral. If the assembly is interpreted as a spiral, the winding sense is counter-clockwise, in agreement with the large scale spiral arms. The colours of the knots are consistent with stellar and nuclear continuum contributions (section 3.2). We explored several methods of removing the low frequency galactic component, including various smoothing filters, a one-dimensional elliptical isophote model, and a multi-component (bulge, disk, point-source) elliptical isophote model. All methods consistently unveil the spiraling structure, with knots coincident in all of *J*, *H*, *K*- and HST *V*-bands. However, in the central 0.5 arcsec of the galaxy, subtracting isophotal fitting models (unsharp masking) reveals prominent artifacts which obscure structural details. as described in Chapman et al. (1999a, 1998).

We note that there has been some controversy over artifacts at the core of AGN galaxies imaged with AO, which imitate expected AGN structures (spiral arms, tori, bars, etc.). Firstly, all structures treated as physical in this paper are either further from the nucleus, or else they are distinctly different and more extended than the artifacts cataloged in Chapman et al. (1998, 1999a). Secondly, we have compared the general morphology with HST-NICMOS images (Alonso-Herrero, private communication), which shows similar features, although at a lower spatial resolution at *K*-band and with $0.1''$ pixels compared with our $0.034''$ pixels.

Colour maps are formed by smoothing the images to the worse resolution of a given pair and taking the flux ratio (figure 3). The colour scheme used has redder colours

darker (red) to emphasize dusty structures. Any colour gradients in these images can result from several different processes: 1) change in the optical depth from dust 2) change in the stellar population 3) change in the gas emission features (primarily $H\alpha$). The most prominent feature is an irregular-shaped patch to the southwest. The fact that this region appears clearly as a deficit in the *V*-band image, and takes on a patchy morphology is strong evidence for dust obscuration as the source of the colour gradient. The region is therefore most pronounced in the *V-K* colour map, since the *K* image is least affected by dust. The *J-K* and *H-K* images indicate that substantial dust still affects this region in the *J*, and even *H*-bands. We estimate $A(V) \sim 8$ magnitudes in this region, assuming an intrinsic stellar index of $H-K=0.22$, $J-H=0.78$ (Glass & Moorwood 1985), and an extinction law $A(K)=0.112 A(V)$, $A(H)=0.175 A(V)$ and $A(J)=0.282 A(V)$ (Rieke & Lebofsky 1985). The colour maps reveal that the nucleus itself is very red, consistent with a reddened nuclear continuum component, with possible thermal dust emission in the *K*-band. The red colours surrounding the region of bright pointlike objects described above stands out from a region slightly bluer than the larger scale bulge of the galaxy. To the northeast, the colours are generally bluer, although this may simply be in contrast to the very red colours of the SW dust absorption. The *J-K*, *H-K* maps reveal that there may be a blue ring with a $2''$ radius.

Although the HST *V*-band image has strong CCD bleeding from the bright nucleus, a northeastern nuclear extension of about $1''$ to the isophotes is apparent in all the images except *K*-band (figure 1). It extends furthest, and with the largest position angle (PA), in the shorter wavelength *V*- and *J*-band images. The feature appears as an ellipse of $\sim 1''$ extent in the colour maps, roughly orthogonal to the plane of the galaxy. This $\sim 45^\circ$ PA feature, has bluer colours ($H-K = 0.10$) than the surrounding regions, including the blue region ($H-K = 0.15$) surrounding the pointlike objects visible in the unsharp masked images (figure 2). Given the difficulty in extinguishing *K*-band light when shorter wavelength light is prominent, a natural explanation is young hot stars near the galaxy core.

The images are distorted by PSF artifacts in the central $0.5''$, plus the above mentioned CCD bleeding in the HST image. However, the extent and position angle (PA) of 43° indicate that this feature is likely unrelated to the AOB artifacts described in Chapman et al. (1999a,1998). Although the HST CCD bleeding lies along a similar PA, the feature appears in all the near-IR colour maps by themselves. Figures 7 and 8 depict all of these structures relative to each other and the larger scale galaxy).

3.2 Colour-colour analysis

The colour-colour diagram of the point-like structures (hereafter called knots) revealed in figure 2 is displayed in figure 4, highlighting the most clearly identified knots between model-subtracted *J*, *H*, and *K* bands images (figure 2). The colours are measured through aperture photometry, where apertures of $0.2''$, $0.3''$ and $0.4''$ were used to derive an estimate for the uncertainty of 0.5 magnitudes for *J-H* and 0.3 magnitudes for *H-K*. The larger uncertainty in the *J-H* index is likely a result of the poorer resolution in *J*-band

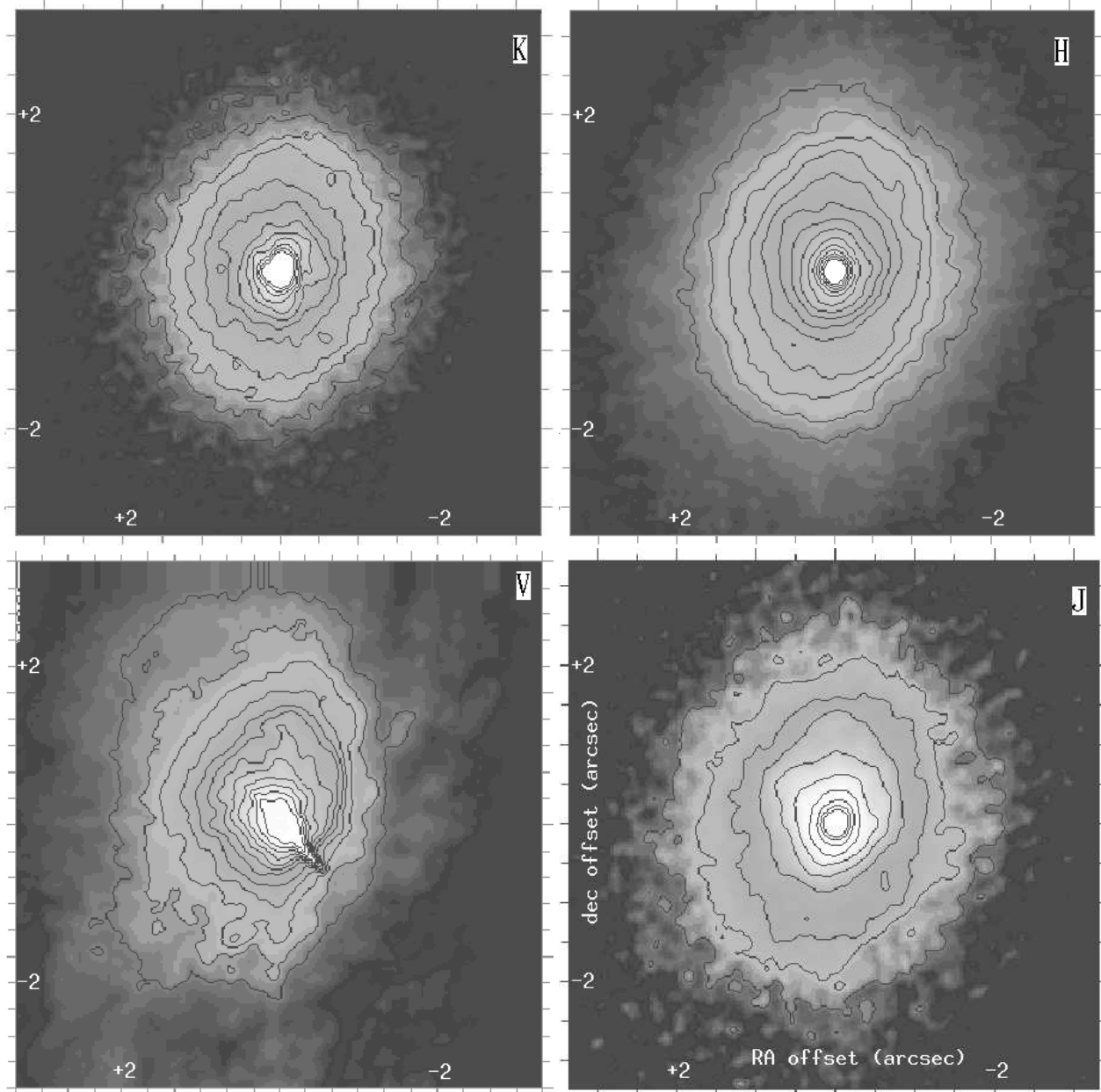


Figure 1. The central $6.7''$ of NGC 3227 in K , H , J , F606W (hereafter V -band). In all images, North is up, East is left. The strong SW/NE feature in the HST V image is due to bleeding/saturation in the nucleus.

relative to H and K , and some of the knot regions blend with surrounding ones. The colours of the regions and visible knots were verified in the actual colour maps, where the estimated photometric accuracy is < 0.3 magnitudes. Within the uncertainty there is still a rather large spread in the colours for these knot structures. The knots further from the nucleus tend to have colours near the locus of normal spiral bulge stars (triangle symbols), while those closer in are more centered on the continuum power law region (square symbols). This can be explained if scattered nuclear light and thermal dust emission are superposed with a star-bursting component for the nuclear knots.

3.3 Isophotal analysis and small-scale bars

The transfer of mass from large to small scales is a vexing problem in AGN research. From a theoretical standpoint, galactic bars are perhaps the most viable candidate for facilitating this mass transfer (Schwartz 1981; Norman 1987; Shlosman, Frank & Begelman 1989). The relatively constant surface brightness along the bar results in a clear signature in the radial profile analysis of a galaxy. We follow the criterion for a nuclear bar discussed in Friedli et al. (1996). This involves a rise then fall in ellipticity (E) while the position angle (PA) stays constant over the rising E . Double bars would appear as two bumps in E , and a bar plus twist has the PA and E (or just PA) changing simultaneously after the

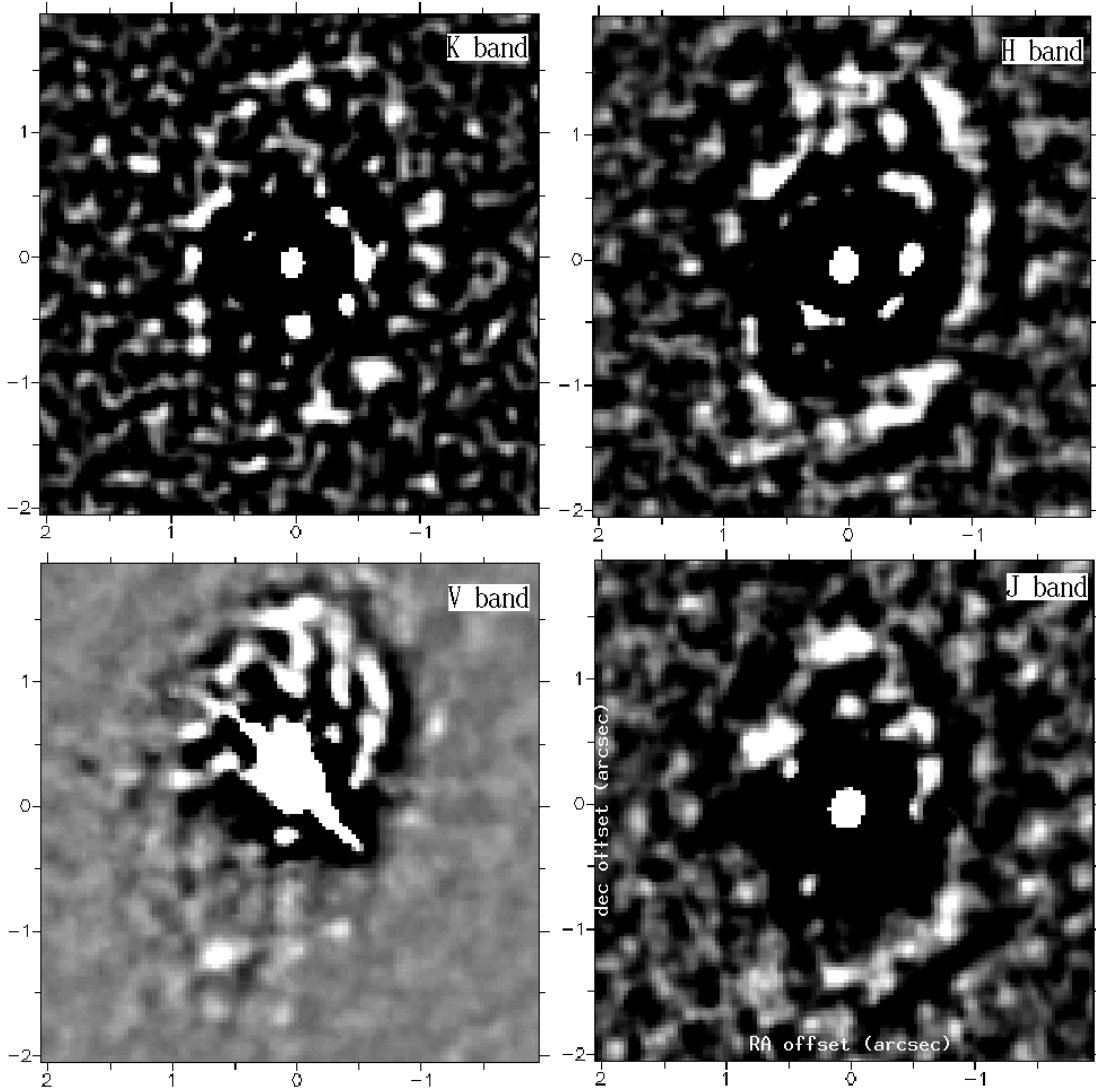


Figure 2. Close-up of central $4''$ region with smooth model subtracted images of NGC 3227. Clockwise from upper left is *K*, *H*, *J*, *V*. See figure 8 for a cartoon of the claimed structure. The strong SW/NE feature in the HST *V* image is due to bleeding/saturation in the nucleus.

Figure 3. Colour maps of NGC 3227, **top row:** *J-K*, *H-K*, **middle row:** *V-K*, *V-H*, **bottom row:** *V-J*. The colour scheme used has redder colours darker, and bluer colours lighter. The strong SW/NE feature in images formed with the *V*-band is due to bleeding/saturation in the nucleus of the HST *V*-band CCD image. A blue ring at $\sim 2''$ radius is apparent in the *J-K*, *H-K* maps, however the effect is largely obscured with the dusty optical HST image.

bump. In the larger scale galaxy, the ellipticity would then decrease to reveal the inclination of the disk, but our field does not extend this far. If there is more than a 10 degree shift in position angle over a bump in E, then the feature is classified as a twisted isophote rather than a bar.

The variations of surface brightness (SB), ellipticity (E), and position angle (PA) for the galaxy were extracted from the fitting of elliptical isophotes. The profiles are similar at *J*, *H* and *K* (figure 5), displaying bumps in ellipticity at $0.5''$ and $1.5''$ radius, confirming the presence and position angle of the nuclear ellipse (PA $\sim 40^\circ$) and the larger enhanced region coincident with the spiral starburst (PA $\sim -10^\circ$).

The *H* and *K* bands are less obscured by dust and the profile is most clearly defined at these wavelengths, whereas the large amount of extinction to the southwest in the *V*-band skews the isophote E and PA fits.

For the spiral knot region ($\sim 1.5''$ radius), the isophotes are twisted of order 10 degrees. The images (figure 1) show that the region extends to the south of the nucleus at *H* and *K* bands and would be consistent with a bar potential by our above criterion. At *V*-band, the region only appears to extend to the north due to the southern dust obscuration.

For the nuclear ellipse, the PA twists more significantly ($\sim 20^\circ$), and its twist and orientation vary with wavelength.

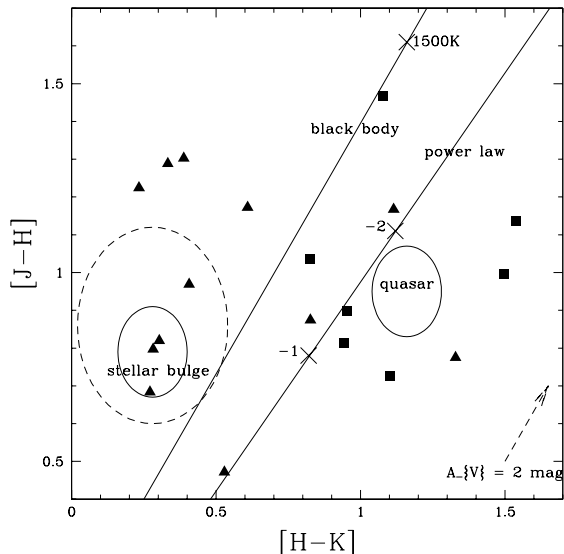


Figure 4. Colour-colour diagram of the knot-like structures in the core region. A vector showing the effects of 2 magnitudes of visual extinction is shown, along with the locus of colours for normal stellar bulges and continuum power law from quasar-type nuclei. The dashed ellipse surrounding the normal bulge colours subsumes our error estimates coupled with younger massive star colours. The knots further from the nucleus ($>0.5''$) tend to have colours near the locus of a stellar bulge (triangle symbols), while those within $0.5''$ are more centered on the continuum power law region (square symbols).

At the smallest scales, this is likely the result of the wavelength dependent AO/PSF artifacts dominating the signal. For the outer extent of the disk, the multiple emission components possibly contributing to the flux (see above) likely vary with wavelength, with a strong stellar component at a larger PA in the J -band. The twisted isophotes do not satisfy our bar criterion, but the profiles are difficult to analyze with certainty as the feature is near the limit of our image resolution and clouded by artifacts in the very core regions.

3.4 Comparison with MERLIN radio data

The images can be compared to the 6 cm and 18 cm MERLIN radio continuum emission (Courtesy of C. Mundell. Originally published in Mundell et al. 1995), which align with the axis of the nuclear spiral (figure 6). Previous explanations for the radio structure (Mundell et al 1995, 1996), invoked the standard unified AGN model to explain this emission. In this standard unified model, a dusty torus preferentially blocks certain views of the active nucleus, and results in anisotropic emission of ionizing continuum photons. The result is a cone-like region of ionized gas, such as [OIII]. Even at the low resolution of their optical images, it was apparent that there was an offset in orientation from an [OIII] ‘‘cone’’ and the small-scale radio features. A projection effect would be possible, but this would necessitate that the NE side of the disc is closer to us than the SW side. This would only be possible if the spiral arms were leading rather than trailing (Mundell et al. 1995, Pedlar et al. 1987).

Our high resolution imaging suggests that the radio emission may be unrelated to any kind of jet outflow, and instead is associated with the nuclear knots observed in figure 2. The peak to the north is only observed at 18cm with no

6cm counterpart, possibly indicating a steep spectrum consistent with supernova remnants in the regions of star formation. The southern peak spectral index is consistent with a compact active nucleus (Mundell 1995, Ho 1999). The absolute positional accuracy of our AOB images was limited to the pointing accuracy of CFHT, and is obviously worse than the VLA. An error of a few tenths of an arcsec is possible in the relative image alignments. We align our near-IR nuclei to the brightest radio peak. Figure 6 indicates that the radio then aligns well with both the orientation and some of the knots of the spiral/ring assembly, and a possible interpretation is that we are seeing synchrotron emission from SNe remnants.

3.5 Unified models and OASIS spectroscopy

The OASIS instrument on the CFHT allows spatially resolved spectroscopy to be obtained at the resolution provided by the Adaptive Optics Bonnette. Spectral imagery was obtained in the $H\alpha$ and [SIII] lines under fairly poor seeing conditions and only part of the data obtained is usable since guiding was lost intermittently in some of the exposures. The best corrected FWHM obtained is only $0.8''$ using the $0.3''$ per pixel sampling. The [SIII] lines are excited under similar conditions to the [OIII] line and is typically $1/3$ the peak intensity. The advantage for adaptive optics is that the PSF correction is much better at 9000 \AA (SIII) than 5000 \AA (OIII).

Initial results from our OASIS data (Chapman & Morris, in preparation) seem to be consistent with the unified model for NGC 3227 proposed in (Gonzalez-Delgado & Perez 1997; Arribas and Mediavilla 1994) providing a higher resolution perspective on the HII region to the southwest, as

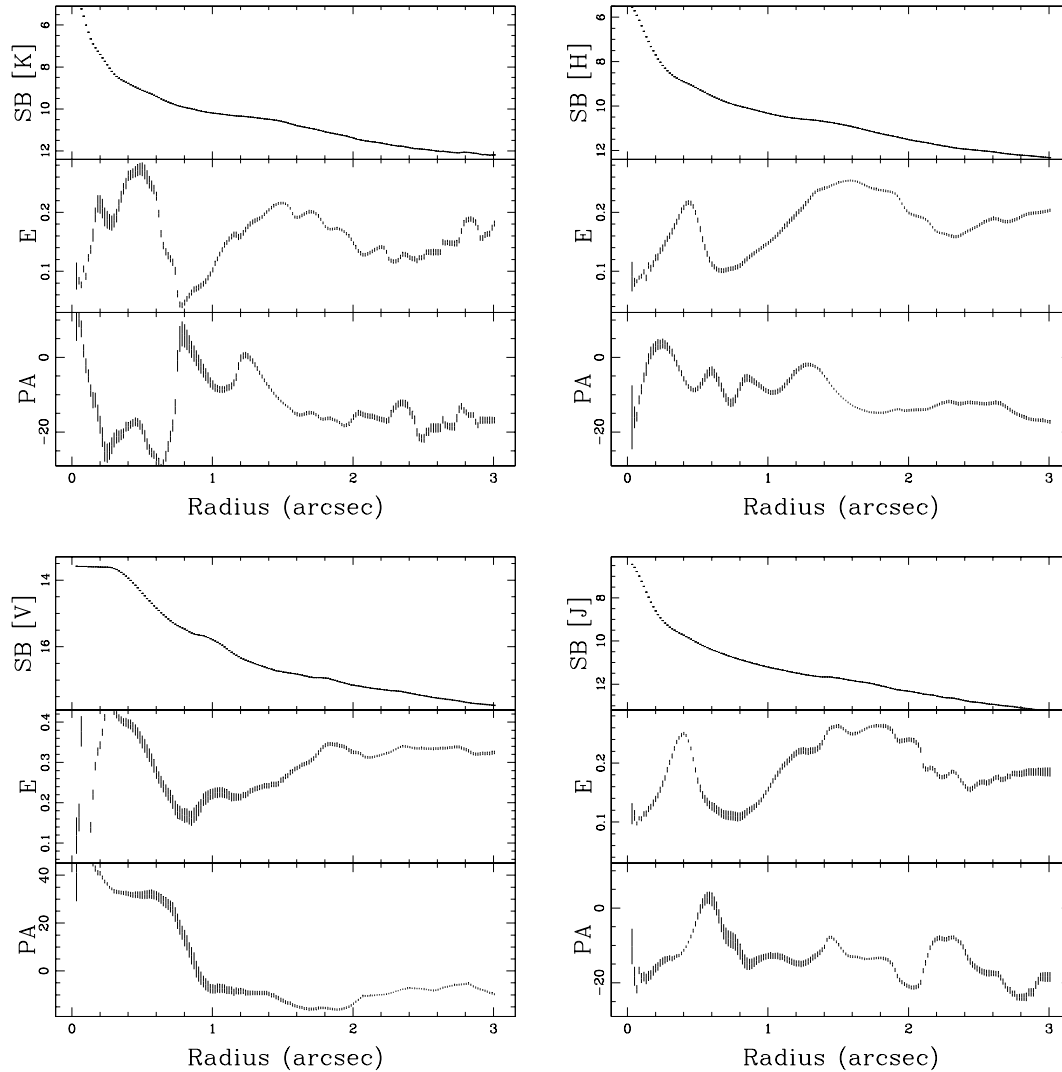


Figure 5. Profiles of NGC 3227 from elliptical isophote fits. Clockwise from upper left: K , H , J , V . The panels (top to bottom) depict surface brightness (SB) in $\text{mag}/\text{arcsec}^2$, ellipticity (E) as $1 - b/a$, and position angle (PA) in degrees from north. Note that the saturated HST V -band surface brightness is flat in the core. Error bars represent 1σ isophote fitting error. The varying position angle over the peaks in ellipticity suggests that there is no clear small-scale bar potential in this Seyfert galaxy.

well as the extended [OIII] and $H\alpha$ to the northeast. The dusty region in the $V-K$ color map falls over the blank region which separates the HII region from the core (Figure 8), likely explaining the disconnected morphology. In the unified AGN picture, biconical emission line regions are thought to be the result of collimated continuum emission via a nuclear dust torus. Although with NGC 3227 one would expect a counterpart to the extended [OIII] emission “cone” on the opposite side of the nucleus (SW), the dusty region would obscure such emission in addition to any $H\alpha$ that extended from the nucleus to the separated HII region.

However, a larger scale extended [OIII] region (Arribas & Mediavilla 1994, Mundell et al. 1995, Gonzalez-Delgado & Perez 1997) lies to the northeast and has been interpreted as a narrow-line region ionized by the AGN, collimated into a cone by a small-scale ($\sim \text{pc}$) dusty torus.

4 DISCUSSION

4.1 Fueling the nucleus

We can then trace the structural components of this galaxy from the largest scales down to the small scales observed in our images (listed in Table 1; cartoons in figures 7 and 8 show a depiction of scales and relationships of the various features). On the largest scales Gonzalez-Delgado & Perez (1997) noted that a large-scale bar appears to transport material towards an inner radius which corresponds to the calculated Inner Linblad Resonance (ILR) at roughly $7''$. At this point, prominent dust and HII regions indicate substantial star formation. Within this region, non-circular motions are observed in the CO rotational transitions by Schinnerer et al. (1999, 2000), using millimeter interferometry at IRAM. The gas motions can be successfully described by a molecular bar or by circular motion in a tilted ring system, characteristic of a warped disk (Schinnerer et al. 2000). The apparent alignment of a possible CO bar with the larger

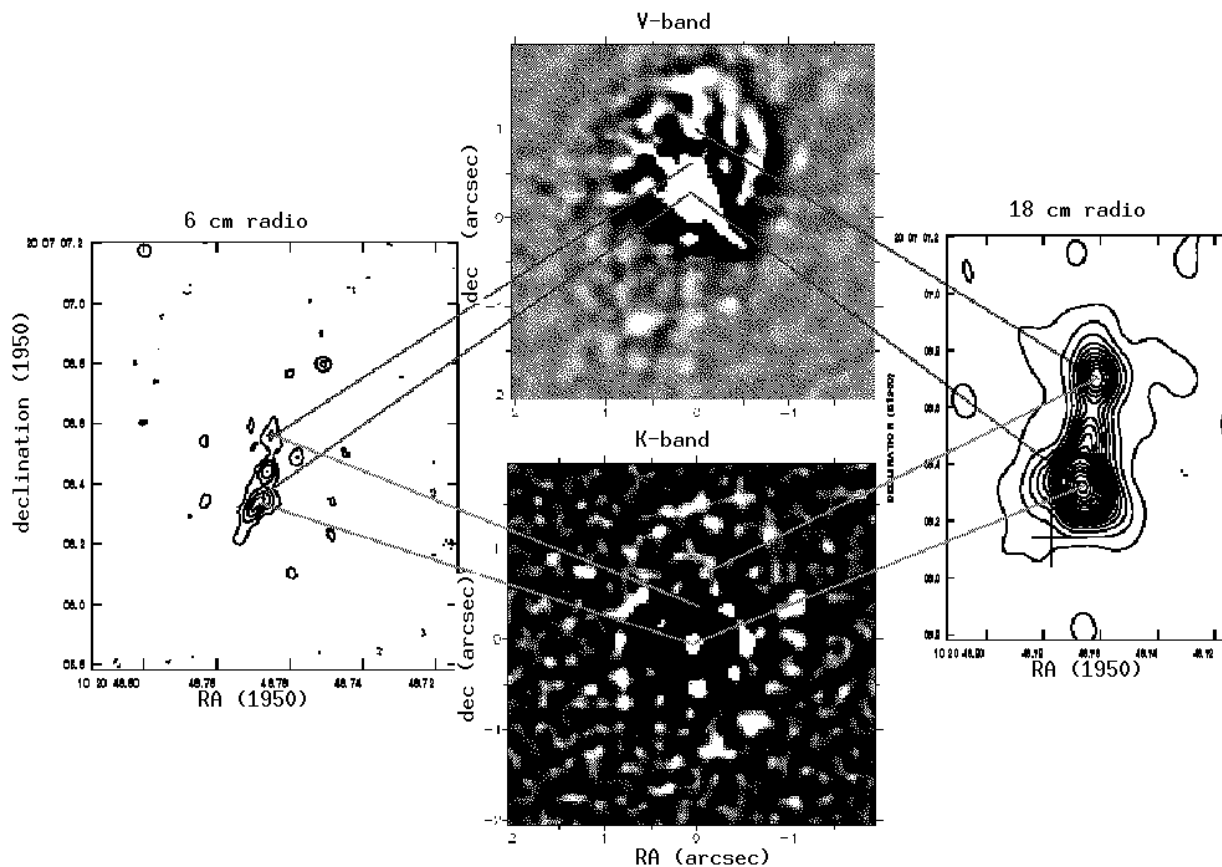


Figure 6. The 6 cm (left contours) and 18 cm (right contours) of NGC 3227 showing the location in the model subtracted V (above) and K (below) bands. Note that there is close alignment of the peaks of the radio maps, with the galaxy core and knot to the north.

optical bar may represent a coupled structure, rather than two kinematically distinct bar potentials (see Friedli 1996, Friedli et al. 1996, 1993 for discussion of nested bar alignment).

The calculated ILR of $\sim 2''$ for a molecular bar model corresponds to the outer extent of our observed ring/spiral of knots (row (7) in Table 1 – see model subtracted images, figure 2) and the blue ring visible in the near-IR colour maps (row (6) in Table 1 – see figure 3). Whether the non-circular molecular gas motions are due to a warped disk or bar, the collected gas at these radii ($2''$) implies recent star formation. The colours of our outer ring/spiral of knots, and the blue $J-K$ ring ($2''$ radius) are consistent with such a star forming scenario.

Our observed smaller scale blue annulus ($J-K$ map – row (10) in Table 1 – see figure 3) extending to a radius of $0''.5$ lies within the warped CO disk in Schinnerer et al. (1999). Our $J-K$ and $H-K$ maps (figure 3) show a red peak $1''$ east of the nucleus which matches the CO intensity peak in Schinnerer et al. (1999), consistent with reddening from the molecular gas. The molecular gas in this region is observed to be counter rotating (Schinnerer et al. 2000), consistent with the warped disk becoming perpendicular to the plane of the galaxy, and our small scale blue annulus may form an inner region of the warped CO disk.

With the bar structure existing at larger scales and extending down to the knotty spiral at $2''$ in our images, along with the torques induced by an even smaller scale warped

disk, it is natural to speculate that the small scale features observed in our images may provide an indication of how material is funneled down to the scales (\sim pc) where viscous forces may take over to fuel the AGN. With a profile analysis (figure 5), both the region of spiral knots and the smaller scale elongation seen in the colour maps are identified as ellipticity peaks. The large amount of twisting in position angle over these peaks indicates that the features are likely not associated with nested bar-potentials. In the absence of any true bar potential in the nuclear region, the fate of knots of star formation generated near the $2''$ ILR would then be to slowly drift inwards with time (Morris & Serabyn 1996), being carried apart by differential rotation. This process could mimic the spiral/ring assembly seen in the core region.

The extended radio feature supports such a fueling picture. Dense blobs spiraling in from 100 's of parsecs due to a viscosity provided by a hot outflowing may provide a means to increase the inflow velocity. However cloud stability is clearly a major problem in this case. In our own galaxy at roughly comparable scales, similar processes are thought to be at work (Morris et al. 1996). Although the Milky Way is thought to have a supermassive black hole in the core (Ghez et al. 1998), it appears not to be active currently, possibly due to lack of fuel, or a means to shorten the inflow timescale.

In certain Seyfert galaxies, Regan and Mulchaey (1999) have found small-scale spiral dust lanes that may be able to

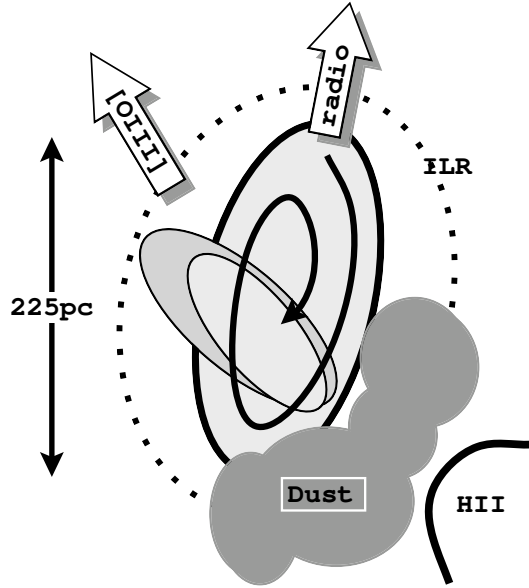


Figure 8. Cartoon of the smaller scale features probed by the CFHT AOB. The ILR of a possible molecular bar (Schinnerer et al. 2000) is depicted as the dashed ellipse surrounding the spiral starburst region. The radio “jet” (PA = -10) aligns with this spiral region. The dusty region to the SW may be a reason for the lack of [OIII] and the detached HII region. The two possible components of the inner nuclear disk/torus are shown as overlapping ellipses (larger PA of the J and V -band isophotes, and smaller PA of the H,K -band isophotes). This may correspond to the inner region of the warped molecular disk in Schinnerer et al. (1999). The direction of the extended [OIII] region is shown by an arrow. The solid black (one-arm) spiral is drawn to suggest the possible structure associated with the nuclear knots seen in figure 2.

provide fuel for the central engine. This is consistent with the results of Chapman et al. (1999c). This suggests that material may indeed be transported inwards by the spiral potential in many AGN, rather than losing its angular momentum in the presence of a strong bar as hypothesized by Shlosman et al. (1989). Our images of NGC 3227 with the spiral knot region would be consistent with this picture. Although it is clear that spiral potentials can transport material inwards (Binney and Tremaine 1987) there has been little theoretical or numerical work to date to support such a scenario. It is not yet clear that the timescales involved could effectively fuel the active nucleus.

A contrary point concerns the fact that the alignment with the axis of the feature described as an [OIII] ionization cone (Gonzalez-Delgado et al. 1997) indicates that our small-scale blue annulus (Table 1, row 10) may represent scattered AGN light. On the other hand, if our observed small-scale elongation is a twisted disk or torus, similar to that found in Centaurus A by Schreier et al. (1998), its plane lies roughly perpendicular to the axis defined by the radio “jet” observed at 6 and 18 cm, and would be consistent with a collimated radio jet normal to an accretion disk plane. For the radio emission to be interpreted as an outflow, the collimated ionization of the NLR picture would then likely have to be abandoned. We explore these scenarios below.

4.2 Unified models and the role of the radio feature

4.2.1 AGN origin to the radio feature

The radio extension may be a jet powered by the Seyfert nucleus. We could then interpret the twisting nuclear ellipse in the central $2''$ as a warped disk/torus related to the collimation axis defined by the radio feature, which we refer to as the *jet* in this section. Several arguments support this picture: (i) there is a molecular disk counterpart at a similar scale with apparent counter rotating gas (Schinnerer et al. 2000); (ii) the near-IR disk/torus is roughly perpendicular to the jet; (iii) the twisting of the disk/torus is in the orientation such that the structure would be more perpendicular with the jet at the smallest scales. The feature might even be associated with an extended torus as seen for instance in NGC 4261 (Jaffe et al. 1996), and as described in the models of Maiolino et al. (1997).

The radio jet aligns well with the north-south elongated region of our knots, and the radio peaks may correspond to knot features. We could interpret this bluer region as a narrow line emission region (NLR) excited by the AGN continuum. Kotilainen et al. (1997) also found a blue excess in their optical colour maps lying in two lobes surrounding the nucleus on the NW-SE axis which they interpreted as scattered nuclear light. Higher spatial resolution spectral imaging is required to confirm whether the line ratios and dynamics within this region are consistent with the continuum ionization of a NLR.

The suggestive spiral/ring morphology of the knots (figure 2) makes it less likely that this region is a random assembly of starburst knots resulting from shocked gas in the NLR/radio jet entrainment. In addition, the nuclear disk may have two emission components at different PA associated as suggested in section 3. Although, within the disk, the more extended ellipse at larger PA certainly appears stellar in origin, the inner disk at smaller PA may be substantially scattered AGN light, implying that the radio jet does not necessarily define a unique collimation axis.

However a small scale (\sim pc) dust torus which collimates the larger scale emission is not a mandatory feature of AGN. Indeed Malkan et al. (1998) have put forth a viable alternative scenario where patchy dust up to 100 pc from the nucleus would lead to the classification differences seen in many AGN (a Galactic Dust Model – GDM). Our near-IR extinction maps for a large sample of Seyfert galaxies show that this is a plausible picture (Chapman et al. 1999c). Cloud-cloud interactions associated with the dense knots observed in our central region may effectively provide a quasi-spherical cloud distribution in this region, providing a natural setting for this model put forth by Malkan et al. 1998. If the GDM describes NGC 3227, then there is not necessarily a contradiction in radio/NLR misalignment: the radio jet extends along the presumed spin axis of the AGN, while the AGN continuum excited emission (NLR) extends anisotropically where it is not obscured by patchy dust – primarily towards the NE.

4.2.2 Starburst origin to the radio feature

Regardless of whether the extended [OIII] narrow-line region to the northeast defines a collimation axis of a small-scale

Table 1
The structural components of NGC 3227, from largest (1) down to the smallest (10)

Component	Scale	PA ($^{\circ}$)	E ($1 - \frac{b}{a}$)	Observed with	Function in galaxy
(1) Large Scale galaxy	1-10 kpc	-22	0.3	V-band	
(2) Large Scale bar	1-5 kpc	-20	0.5	galaxy subtracted	funnel material to ILR at $7''$
(3) Extended [OIII]	1kpc	35		OIII filter/ OASIS [SIII]	collimated emission ?
(4) Circum-nuclear ring	1 kpc			$H\alpha$	ILR
(5) Medium scale bar	100-1000pc	-16		submm CO	funnel material to ILR at $2''$
(6) Blue ring	300 pc	n/a	0	colour maps, esp. $J-K$	young stars?
(7) knots in spiral/ring	200 pc	-10	0.2	model subtract, colour maps	spiral starburst, ILR
(8) $V-K$ ellipse	200 pc	-10	0.1	$V-K$ map, raw V	bluer than galaxy
(9) Radio jets/blob	100 pc	-10		MERLIN 8/16cm	SN/outflow?
(10) $J-K$ annulus	100 pc	40	0.3	all colour maps & images	twisted disk/bars, scattered AGN light

Figure 7. Palomar Digital Sky Survey (DSS) image of NGC 3227 interacting with the dwarf elliptical companion NGC 3226 to the North. Inset cartoon of the larger scale features: the large scale stellar bar funnels material to the ILR (depicted by the large circular region). A proposed smaller-scale molecular bar or warped disk (Schinnerer et al. 2000) resides within (PA is approximate), presumably transporting material down to the scales probed with our AO images (overlapping ellipses in the very core). The [OIII] ionization cone and detached HII region are shown to scale.

obscuring torus, there does seem to be evidence for preferential continuum ionized emission towards the NE regions. The scattered light interpretation of at least part of the disk feature is consistent.

A case can therefore be put forth that there is a “classical” bi-conical emission structure in this galaxy, largely obscured to the SW, and collimated at small scales by some kind of dusty torus. The elliptical region surrounding the starburst knots might then represent a disk, orthogonal to the ionization axis, with well defined spiral arms and small-scale bar, facilitating mass transfer to the core region. With this geometry, in addition to the radio morphology extending along the axis of the ellipse of knot structures (figure 6) (possibly with knots coincident with the actual radio peaks), the most plausible explanation for the radio emission seems to be supernova remnants associated with the starforming clumps. If we accept this picture, it is difficult to interpret the radio feature as an AGN-driven jet mis-aligned with the ionization cone, since projection effects are not consistent with the known motions of the galaxy (Mundell et al. 1995). It does not necessarily preclude an outflow driven by starburst superwinds (Heckman et al. 1990, Unger et al. 1987), since the superwind outflows are preferentially blown out of the plane of the galaxy, consistent with the galactic motions with the SW side of the disk being closer to us than the NE side. An AGN collimation axis would not be expected to lie in any preferred direction (Malkan et al. 1998) and there is no problem interpreting the ionized regions within this geometric picture.

5 CONCLUSIONS

We have observed NGC 3227 at J , H , and K bands using adaptive optics on the CFHT. Despite artifacts surrounding the cores of bright point sources with adaptive optics, we are confident that we have identified several structures in the central few arcseconds. An assembly of knot structures lying in a spiral/ring pattern within a $2''$ radius is suggestive

of embedded spiral arms within the larger-scale spiral of the outer galaxy. With the recent discovery of spiral dust lanes in many Seyfert galaxies observed with HST-NICMOS (Regan & Mulchaey 1999), we suggest that our observed spiral structure may be a fueling mechanism for the AGN.

An elongation of PA $\sim 40^{\circ}$ may be an unresolved continuation of the spiral pattern, or a nuclear disk. The coincidence of this feature within the counter rotating molecular gas suggests the inner warped disk proposed by Schinnerer et al. (2000) as an interpretation. The fact that the elongation aligns fairly well with a larger scale [OIII] extended emission line region, and has rather blue colours, suggests scattered nuclear continuum emission may also be responsible. The extended radio feature observed with MERLIN is, however, not aligned with the [OIII] axis, and is coincident with knot structures in the spiral/ring region.

It is probably true that there must be a variety of mechanisms responsible for ultimately getting gas into the central parsec of an active galaxy. Dense blobs spiraling in from 100’s of parsecs due to a viscosity provided by a hot outflowing may be one possibility, though cloud stability is clearly a major problem in this case. Cloud-cloud interactions may also play a role and effectively provide a quasi-spherical cloud distribution in this region, providing a natural setting for Malkan’s galactic dust model (GDM) unification scenario.

There are still several conflicting pictures which appear consistent with the data. The situation will be further elucidated by higher spatial resolution imaging spectroscopy and perhaps imaging of even smaller-scale morphology with adaptive optics on large telescopes.

ACKNOWLEDGMENTS

The research of SCC and GAHW was supported by a grant to GAHW from the Canadian Natural Sciences and Engineering Research Council. We would like to thank the staff at CFHT for facilitating these observations. We acknowledge

valuable comments from G. Fahlman, D. Scott, M. deRobertis, and an anonymous referee.

REFERENCES

- Alonso-Herrero A., Simpson C., Ward M.J., Wilson A.S., 1998, *ApJ*, 495, 196
- Antonucci R., 1993, *A&AAR* 31, 473
- Arribas S., Mediavilla E. 1994, *ApJ*, 437, 149
- Binney J., Tremaine S., “Galactic Dynamics”, Princeton University Press, Princeton, New Jersey, USA, 1987
- Chapman S.C. Walker G.A.H. & Morris S.L., 1998, *Astronomy with Adaptive Optics*, Proceedings, Sonthofen, Germany.
- Chapman S.C. 1999a, *PASP*, submitted
- Chapman S.C., Morris S.L., Alonso-Herrero A., Falcke H., 1999b, *MNRAS*, in press.
- Chapman S.C., Morris S.L., Walker G.A.H., 1999c, *MNRAS*, Submitted.
- Falcke, H., Wilson A., Simpson C., 1998, *AJ*, 95, 1689
- Friedli D. 1996 *A&A*, 312, 761
- Friedli, D., Wozniak, H., Rieke, M., Martinet, L. & Bratschi, P. 1996, *A&A Supl*, 118, 461
- Friedli, D., Benz, W., 1993 *A&A*, 268, 65
- Ghez A.M., Klein B.L., Morris M., Becklin E., 1998, *ApJ*, 509, 678, (astro-ph/9807210)
- Glass and Moorwood, 1985, *ApJ*, 214, 429
- Gonzalez-Delgado R.M., Perez E. 1997, *MNRAS*, 284, 931
- Heckman, T. M., Armus, L., Miley, G. K. 1990, *ApJS*, 74, 833
- Ho L., 1999, *ApJ*, 510, 631 (astro-ph/9809145)
- Jaffe W., et al., 1996, *ApJ*, 460, 214
- Knapen J., Laine S., Yates J., Robinson A., Richards A., Doyon R., Nadeau D., 1997, *ApJ*, 490L, 29
- Kotilainen J. & Ward M., 1997, *A&AS*, 121, 77
- Lai O., Rouan D., Rigaut F., Arsenault R., Gendron E., 1998, *A&A*, 334, 783
- Malkan M., Gorjian V., Tam R., 1998, *ApJS*, 117, 25
- McLeod, K. and Rieke, G. 1995, *ApJ*, 464, 641
- Morris M., Serabyn E., 1996, *ARA&A* 34 645
- Mundell C.G., Holloway A., Pedlar A., Meaburn J., Kukula M., Axon D., 1995, *MNRAS*, 275, 67
- Mundell C.G., Pedlar A., Meaburn J., Axon D., Unger S., 1996, *MNRAS*, 277, 641
- Nadeau D., Murphy D.C., Doyon R., Rowlands N., 1994, *PASP*, 106, 909
- Norman, C. 1987, in *Galactic and Extragalactic Star Formation*, (eds. Pudritz, R. E. & Fich, M.), Kluwer, Dordrecht, p 495.
- Regan M., Mulchaey J., *AJ*, 1999, 117, 2676
- Rieke M. and Lebofsky A. 1985, *ApJ*, 288, 618
- Rigaut F., Salmon D., Arsenault R., Thomas J., Lai O., Rouan D., Veran J-P., et al., 1998, *PASP*, 110, 152
- Roddier F.J., Graves J.E., McKenna D., Northcott M.J. , 1991, *proceedings of spie* Vol. 1524, p. 248
- Rouan D., Rigaut F., Alloin D., Lai O., Doyon R., Crampton D., Gendron E., Arsenault R., 1998, *A&A*, 339, 687.
- Schreier E.J., Marconi A., Axon D., Caon N., Macchetto D., Capetti A., Hough H., Young S., Packham C., 1998, *ApJ*, 499L, 143
- Schinnerer E., Eckart A., Tacconi L., 1999, *ApJ*, 524, L5
- Schinnerer E. Eckart A., Tacconi L., 2000, *ApJ*, in press
- Shlosman, I., Frank, J., & Begelman, M. 1989, *Nature*, 338, 45
- Schwartz, M. 1981, *ApJ*, 247, 77
- Ulvstad J., Wilson A. 1984, *ApJ*, 285, 439
- Unger, S. W., Pedlar, A., Axon, D. J., Whittle, M., Meurs, E. J. A., Ward, M. J., 1987 *MNRAS*, 228, 671
- Véran J.P., Rigaut F., Maître H., Rouan D., 1997, *Journ. of the Optic. Soc. of America A* 14, 11

This figure "m3hvC.gif" is available in "gif" format from:

<http://arxiv.org/ps/astro-ph/9912032v1>

This figure "m3jvC.gif" is available in "gif" format from:

<http://arxiv.org/ps/astro-ph/9912032v1>

This figure "m3khC.gif" is available in "gif" format from:

<http://arxiv.org/ps/astro-ph/9912032v1>

This figure "m3kjC.gif" is available in "gif" format from:

<http://arxiv.org/ps/astro-ph/9912032v1>

This figure "m3kvC.gif" is available in "gif" format from:

<http://arxiv.org/ps/astro-ph/9912032v1>

This figure "n3big.gif" is available in "gif" format from:

<http://arxiv.org/ps/astro-ph/9912032v1>